A Spatially Variable Time Series of Sea Level Change Due to Artificial Water Impoundment

William B. Hawley[1,2,†], Carling C. Hay[3], Jerry X. Mitrovica[4], and Robert E. Kopp[5]

[1]Department of Earth and Planetary Science, University of California, Berkeley, Berkeley, CA 94720, USA.

[2]Berkeley Seismological Laboratory, 215 McCone Hall, University of California, Berkeley, Berkeley, CA 94720, USA.

[3]Department of Earth and Environmental Sciences, Boston College, Chestnut Hill, MA 02467, USA.

[4]Department of Earth and Planetary Sciences, Harvard University, 20 Oxford Street, Cambridge, MA, 02138, USA.

[5]Department of Earth and Planetary Sciences and Rutgers Institute of Earth, Ocean, and Atmospheric Sciences, Rutgers University, New Brunswick, NJ 08901, USA

Corresponding author: William Hawley (whawley@ldeo.columbia.edu)

[†]Now at Lamont-Doherty Earth Observatory of Columbia University, 61 Rte. 9W, Palisades, NY 10964, USA.

Key Points:

- We present a spatially-resolved time series of sea level due to reservoir construction from 1900 – 2040.

- Some locations in the past century have experienced a reservoir-induced rise in sea level that exceeds 40 mm over less than a decade.

- Future dam construction will cause patterns in sea level change that are different from the past, and larger than current projections.

24 **Abstract**

25 The artificial impoundment of water behind dams causes global mean sea level (GMSL) to fall
26 as reservoirs fill, but also generates a local rise in sea level due to the increased mass in the
27 reservoir and the crustal deformation this mass induces. To estimate spatiotemporal fluctuations
28 in sea level due to water impoundment, we use a historical data set that includes 6,329 reservoirs
29 completed between 1900 and 2011, as well as projections of 3,565 reservoirs that are expected to
30 be completed by 2040. The GMSL change associated with the historical data (-0.2 mm yr^{-1} from
31 1900 – 2011) is consistent with previous studies, but the temporal and spatial resolution allows
32 for local studies that were not previously possible, revealing that some locations experience a sea
33 level rise of as much as 40 mm over less than a decade. Future construction of reservoirs through
34 ~2040 is projected to cause a GMSL fall whose rate is comparable to that of the last century ($-$
35 0.3 mm yr^{-1}), but with a geographic distribution that will be distinct from the last century,
36 including a rise in sea level in more coastal areas. The analysis of expected construction shows
37 that significant impoundment near coastal communities in the coming decades could enhance the
38 flooding risk already heightened by global sea level rise.

39 **Plain Language Summary**

40 Filling a reservoir prevents that water from flowing back to the ocean, thus causing sea level to
41 fall. But sea level does not change by the same amount everywhere: the mass of the water in the
42 reservoir causes sea level to rise in locations near the reservoir, but fall in locations that are
43 farther away. We use databases that include the locations and capacities of reservoirs to estimate
44 how constructing reservoirs has changed sea level, and explore how these changes have varied in
45 space and in time. We find that while constructing reservoirs since 1900 has caused sea level to
46 fall on average, there are some locations that experience a dramatic sea level rise, as much as 40
47 mm, over a short period of time, usually only a few years. As more reservoirs are built, we
48 expect this trend to continue. In fact, reservoirs that are currently being planned—if completed—
49 will generate a sea level rise of a few millimeters in some low-lying coastal areas. This rise
50 would be in addition to the rise in sea level from many other known factors.

51 **1 Introduction**

52   Global and regional changes in sea level are driven by a wide range of processes,
53 including the redistribution of mass from melting glaciers and ice sheets, the continued
54 adjustment of the solid Earth to ice mass changes during the last glacial period, steric expansion
55 of ocean water, ocean circulation changes, and both natural and artificial changes in terrestrial
56 water storage (Cazenave *et al.*, 2018; Kopp *et al.*, 2015). Proper characterization of each of these
57 different components of the sea level budget is necessary for accurate projections of future
58 changes in sea level. In this context, the role of terrestrial water storage remains underexplored
59 and serves as the focus of the present study. We provide the most complete picture to date of the
60 impact that artificially impounded water has had on sea level over the last century, resolved both
61 spatially and temporally, and an estimate of future sea level changes due to projected reservoir
62 construction.

63   Chao *et al.* (2008) use the International Commission on Large Dams World Register of
64 Dams (WRD) (www.icold-cigb.org) database to construct an estimate of the global mean sea
65 level (GMSL) change due to the construction of 29,484 reservoirs worldwide. They estimate the
66 total volume of impounded water to be 10,800 km^3, corresponding to a GMSL fall of ~0.55 mm

67 yr^{-1} in the half century prior to their publication. Sea level changes associated with the
68 impoundment of water on land will be geographically variable (Fiedler and Conrad, 2010) and
69 each reservoir will have a unique sea level "fingerprint," or gravitational, rotational, and
70 deformational (GRD) response to mass redistribution (Gregory *et al.*, 2019). The redistribution
71 of water from the ocean to the reservoir will (1) increase the gravitational attraction of the
72 reservoir on the surrounding water and thus raise the local sea surface height, (2) induce a
73 change in Earth's moment of inertia, and (3) drive local crustal subsidence. Indeed, relative sea
74 level (RSL) will rise within ~2000 km of a reservoir being filled, despite a drop in GMSL, and it
75 will fall by increasing amounts at larger distances from the source of impoundment. The local
76 signal, which can have a peak value an order of magnitude larger than the GMSL change
77 associated with the impoundment, is primarily a result of processes (1) and (3). Calculating the
78 global sea level pattern associated with water impoundment requires knowledge of both the size
79 and location of a reservoir.

80   The WRD database adopted by Chao *et al.* (2008) includes the largest global tabulation
81 of reservoirs and the most complete estimate of the total volume stored in those reservoirs.
82 However, it does not provide locations for these reservoirs and thus cannot be used to generate
83 maps of the associated sea level change. To compute such a map, Fiedler and Conrad (2010)
84 adopt a dataset (Vörösmarty *et al.*, 1997) that includes the locations of 674 reservoirs currently
85 built and scale their result upwards to match the GMSL cited by Chao *et al.* (2008). We extend
86 their analysis in three ways. First, we make use of a much larger database of reservoirs. Second,
87 we explore both the spatial and temporal patterns of RSL change associated with water
88 impoundment. Finally, we project the signals into the future using a database of planned dam
89 construction (Zarfl *et al.*, 2015).

90 **2 Reservoir Databases**

91   In the present study, we use two different databases of reservoir construction. For the
92 time period 1900 – 2011, we use the Global Reservoir and Dam (GRanD) database (Lehner *et*
93 *al.*, 2011), which aims to geospatially reference all reservoirs with a capacity of more than 0.1
94 km^3. It contains 6,329 reservoirs that were completed after 1900 and reports their location, year
95 of construction, and capacity (Fig. 1a). The total volume of these reservoirs is 5,979 km^3, which
96 is less than 8,300 km^3, as reported in the WRD (Chao *et al.*, 2008). Time series of integrated
97 water volume impoundment (and equivalent GMSL fall) for the GRanD database is shown in
98 Fig. 2 (blue histogram). Although the GRanD database contains only ~72% of the volume
99 reported in the WRD, we do not scale our total impounded water volume to match the WRD
100 values because the primary purpose of this study is to estimate the spatial variability of sea level,
101 and water impoundment not included in the GRanD database has an unknown geographical
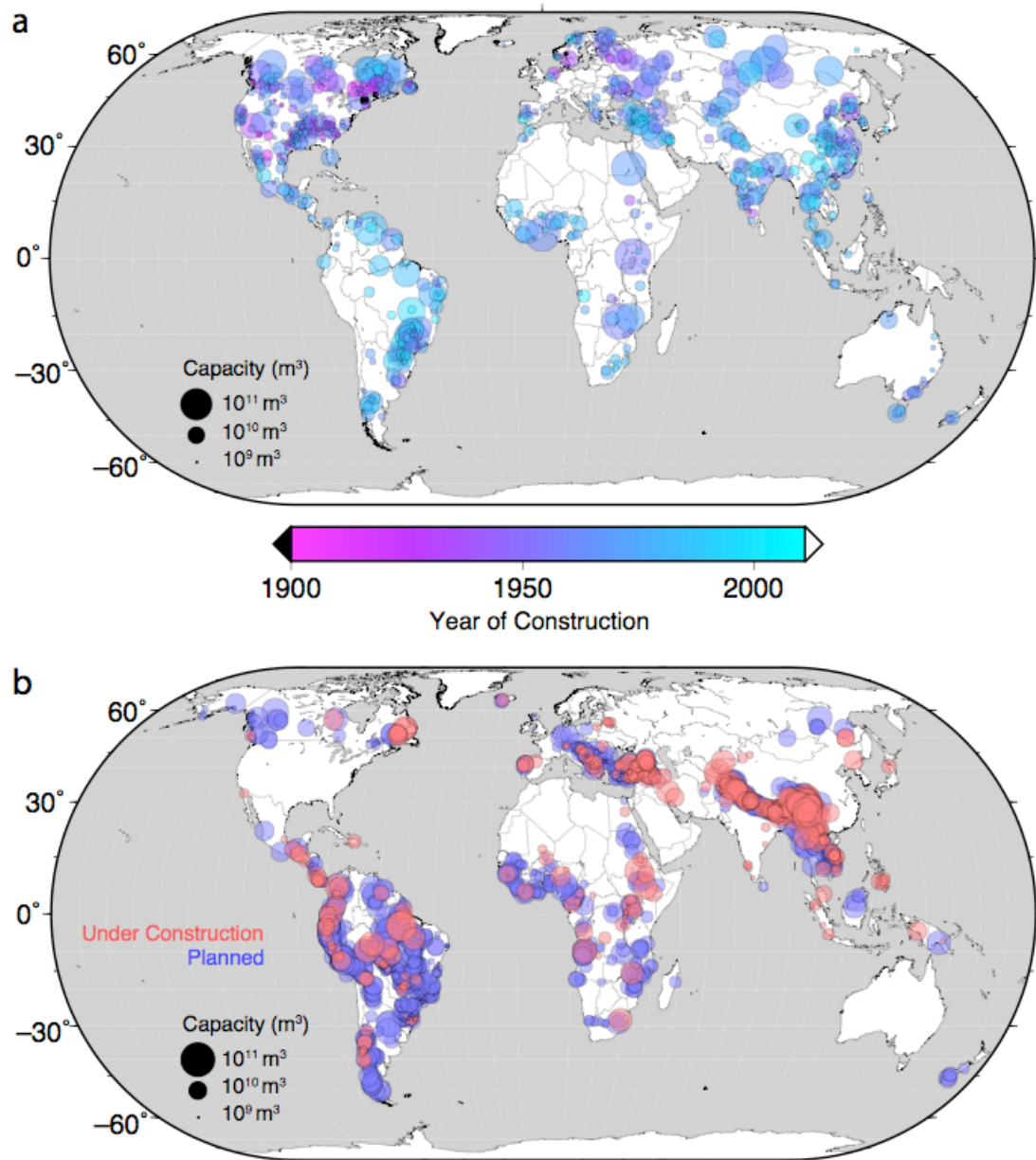102 distribution.

Figure 1. Map of reservoirs and their capacities. Global maps of reservoir locations, with the size of symbols corresponding to (log) capacity, and color corresponding to year of completion. Only larger reservoirs are plotted. (**a**) shows the GRanD database (Lehner *et al.*, 2011); (**b**) shows the database of Zarfl *et al.* (2015).

108

109   In the GRanD database, standard filling rates suggest that we can assume that the smaller
110   reservoirs filled over the course of a year. However, the same is not true for the largest reservoirs
111   in the database. In the case of the largest nine reservoirs, we use various records of the filling
112   duration or average discharge rate (e.g., Loo, 2007) and assume a steady filling rate. For these
113   nine largest reservoirs, the average volume added per year is approximately 23 km^3. The 49
114   largest reservoirs in GRanD database have a capacity larger than 23 km^3, and for all these
115   reservoirs we adopt a filling rate of 23 km^3 yr^{-1}. Each reservoir smaller than this is assumed to
116   have filled the year the dam was completed. These filling rates are accounted for in the time
117   series of Fig. 2.

118   For the future projections, we use a database compiled by Zarfl *et al*. (2015), which
119   includes dams that will be built for hydropower and whose power generation capacity exceeds 1
120   MW (Fig. 1b). The dataset contains no direct information on the expected impounded volume of
121   each reservoir; however, it lists the planned hydroelectric capacity. We use this value to estimate
122   the impounded volume, following Grill *et al*. (2015):

123                      $$V = (3.19 \times 10^6 \text{ m}^3 \text{ MW}^{-1})\,P \qquad\qquad (1)$$

124   where V is the reservoir volume and P is the power generation capacity. Furthermore, because
125   these dams were not complete at the time of the publication of Zarfl *et al*. (2015), many do not
126   have an estimated year of completion. Instead, 3,565 reservoirs are listed as being in one of two
127   broad categories, either in the construction phase (n = 501, or 15% of the total) or the planning
128   phase (n = 2894, or 85%). Using these categories, and the equation above, we estimate that the
129   reservoirs under construction will impound 663 km^3 and that those being planned will contribute
130   an additional 1,500 km^3. Adding these values to results for the GRanD database yields the time
131   series of integrated water volume impoundment shown in the inset to Fig. 2, assuming, following
132   Zarfl *et al.* (2015), that all dams will be completed by the year 2040 (blue histogram).

133   **3 Results**

134   3.1 *Temporal Variation in GMSL*

135   Removing 5,979 km^3 of water from 1900 to 2011 according to the GRanD database
136   corresponds to a GMSL fall of 16.6 mm, or an average 0.15 mm yr^{-1}. As noted above, these
137   values are 72% of the 23 mm and 0.21 mm yr^{-1} reported in Chao *et al*. (2008). Impounding the
138   663 km^3 (under construction) and 1,500 km^3 (planned) from the Zarfl *et al*. (2015) database will
139   cause a further globally averaged drop in sea level of 1.8 mm and 4.2 mm, respectively, for a
140   total of 6 mm. Thus, over the period 2020 – 2040, the mean GMSL rate associated with water
141   entering reservoirs will likely be –0.3 mm yr^{-1}, which is larger than the average rate that occurred
142   over the past century.

143   The above numbers will increase when accounting for natural seepage of water into the
144   land surrounding the reservoir. After a reservoir is built, water will slowly seep into the
145   neighboring land. As this occurs, the flow of water into the reservoir continues to recharge it, but
146   the water that seeps from the reservoir remains relatively localized and does not generally reach
147   the ocean, adding to the total impounded water. While the rate of seepage depends on numerous
148   local factors (*e.g*., Harr, 1962), for simplicity we follow Chao *et al*. (2008) and use a single
149   equation to estimate the seepage rate at each reservoir:

150 $$V(t) = 0.05 \, V_0 \, t^{1/2} \qquad\qquad\qquad (2)$$

151 where V_0 is the reported volume of the reservoir, t is the time in years since the water was
152 impounded, and $V(t)$ is the total amount of water that seeps by time t. According to this equation,
153 seepage contributed an estimated 1,878 km^3 of water by 2011, for a total impounded volume of
154 7,857 km^3. This corresponds to a total GMSL drop of 21.8 mm from 1900 – 2011 (Fig. 2, red
155 histogram in main frame and inset). By 2040, we estimate that this value will increase to 30.1
156 mm, assuming for the seepage term that every "under construction" reservoir is completed by
157 2025, and every "planned" reservoir is completed by 2035. (We make the assumption that, for
158 example, every "planned" reservoir is constructed in the decade 2030 – 2039; assigning every
159 "planned" reservoir to the year 2039 will result in a seepage rate that is too low. We choose a
160 date in the middle of the decade to give the best sense of the GRD fingerprint including seepage.)

161   Analysis of the GRanD time series indicates that the GMSL time series is characterized
162 by markedly different rates in three distinct time windows: from 1900 to 1949 the volume of
163 impounded water rose gradually; from 1950 to 1979 the rate of water impoundment increased
164 dramatically, and from 1980 to 2011, new construction slowed but seepage became increasingly
165 significant. Predictions from the Zarfl *et al.* (2015) database show a further dramatic increase in
166 water impoundment in the next two decades. Many of these reservoirs will be near the coast (Fig.
167 1b), so a complete characterization of the effect this impounded water will have on sea level will
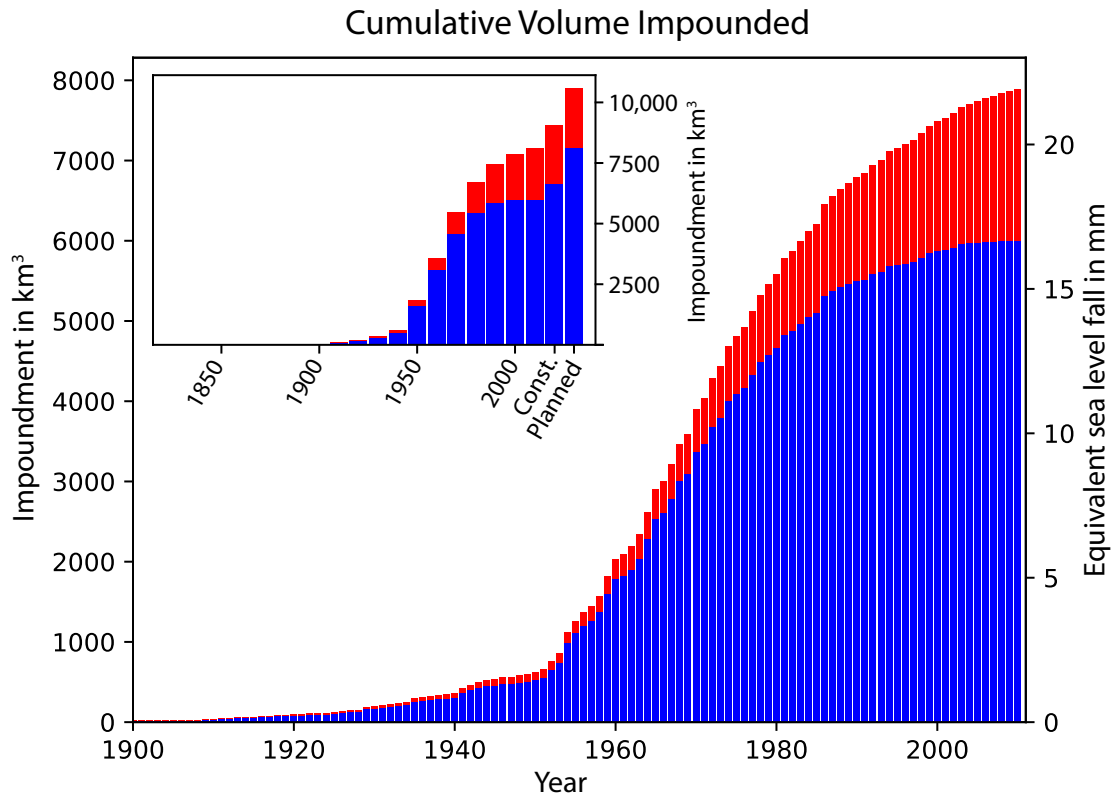168 help refine coastal hazard assessment.

169

170   **Figure 2**. Histogram of total volume of water impoundment. Main figure: Total
171   integrated volume of water impounded as a function time based on the GRanD database

172 without (blue) and with (red) seepage considered. Right axis shows the equivalent GMSL
173 fall associated with the impoundment. Inset: Extension of both curves in the main figure
174 to include projected water impoundments for reservoirs under construction ('Const.') and
175 Planned. Seepage for the column labeled 'Const.' is estimated only from the GRanD
176 database to the year 2025. Seepage for the column labeled 'Planned' is estimated from
177 the GRanD database to the year 2035, plus ten years of seepage from those reservoirs in
178 the "under construction" category.

179 3.2 *Spatial Variation in Sea Level*

180 For each of the 9,724 records in our combined database, we generate a gravitationally
181 consistent prediction of the GRD fingerprint by solving a version of the so-called sea level
182 equation (Farrell and Clark, 1976) that includes the feedback into sea level of impoundment-
183 induced perturbations in the Earth's rotation vector and shoreline migration (Mitrovica and
184 Milne, 2003), although the latter is negligible in the calculations performed here. The results are
185 generated using the pseudo-spectral algorithm of Kendall *et al*. (2005) applied to a 1-D elastic
186 Earth model in which an initial guess to the fingerprint is iteratively improved until convergence
187 is reached. Three such iterations are generally sufficient to establish convergence. Mitrovica *et*
188 *al.* (2011) have shown that our neglect of lateral variations in mantle density and elastic
189 constants, which is motivated by the high computational requirements of 3-D simulations,
190 introduces a small, 1% error in the fingerprints. We adopt the depth-varying elastic and density
191 structure reported by the seismically inferred Preliminary Reference Earth Model (Dziewonski
192 and Anderson, 1981) and the calculations are based on a spherical harmonic truncation at degree
193 and order 512. Test calculations at tide gauge sites using a spherical harmonic truncation level of
194 1024 show negligible differences with those reported below.

195 An example GRD fingerprint is shown for Manicouagan Reservoir (the sixth largest in
196 our dataset, with a capacity of 162 km^3) in Fig. S1. The amplitude of the sea level rise close to
197 the reservoir exceeds the GMSL changes associated with this impoundment by over an order of
198 magnitude, and the zone of predicted sea level rise extends ~2000 km from the location of the
199 reservoir. In the far-field of the reservoir the predicted sea level fall reaches an amplitude ~35%
200 greater than the GMSL change. Moreover, the signal due to rotational effects is evident in the
201 global fingerprint (note in Fig. S1 the decreased magnitude south of Australia and the increased
202 magnitudes over eastern Asia and southern South America).

203 In the absence of significant shoreline migration, the computed GRD fingerprints add
204 linearly. Taking advantage of this linearity, we have constructed a net sea level fingerprint for
205 every calendar year, accounting for the various time series of reservoir impoundment and
206 seepage rates. Fingerprints for a selected set of years are shown in Fig. 3. The full suite of annual
207 fingerprints for the period 1900 – 2011 is available at doi.org/10.5281/zenodo.3751986. A
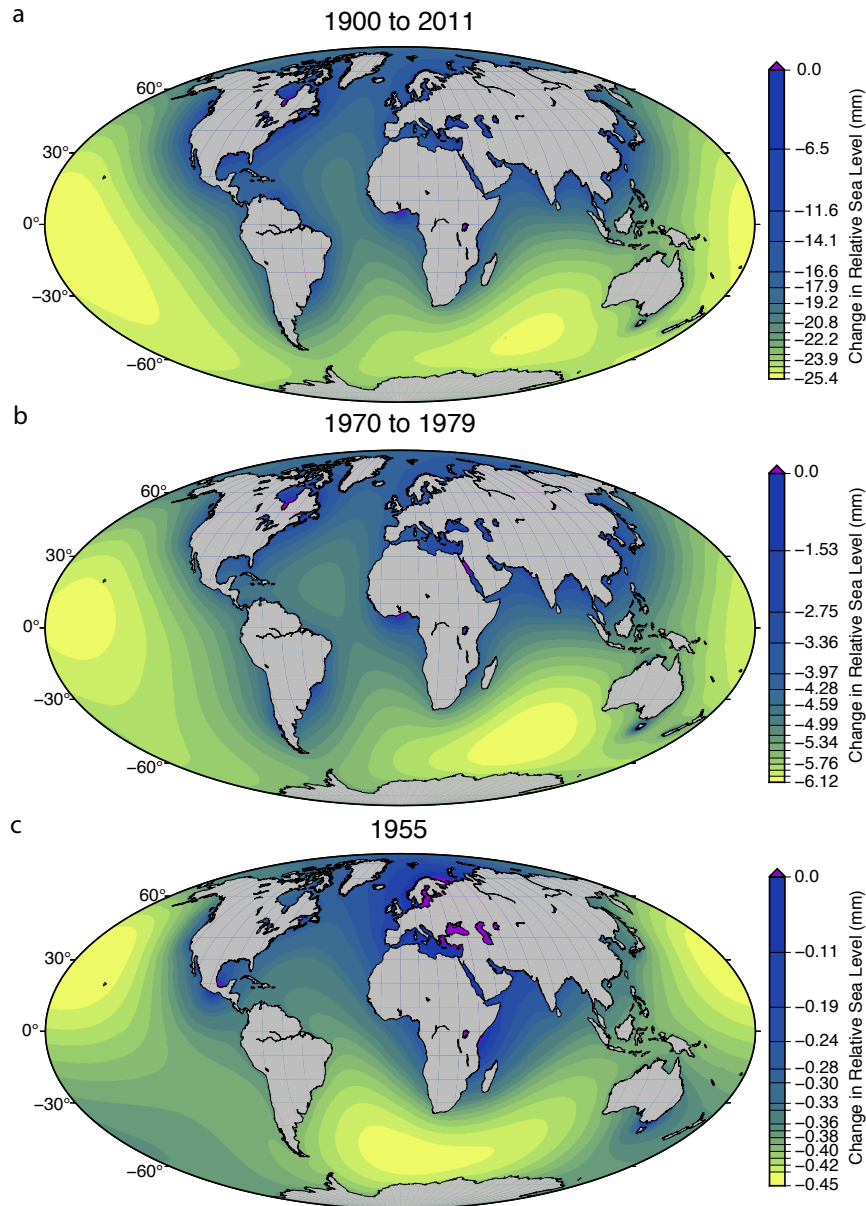208 comparison with the fingerprint of Fiedler and Conrad (2010) is shown in Fig. S2.

Figure 3. Sea level GRD fingerprints over various time periods showing the relative sea level change as a result of reservoir construction including seepage. In each plot, the color bar is scaled to the maximum sea level fall. (**a**) Combined fingerprint of all reservoirs in the GRanD database (1900 – 2011), including seepage. (**b**) Fingerprint of all water impounded in the decade 1970 – 1979, a period of prolific dam construction. (**c**) Fingerprint of all water impounded during the year 1955.

The GRD fingerprints for the future construction from the database of Zarfl *et al.* (2015) are shown in Fig. 4. The global signal (Fig. 4a) shows a markedly different geographic distribution than the GRanD database (Fig. 3a), notably in northern South America and Southeast Asia.
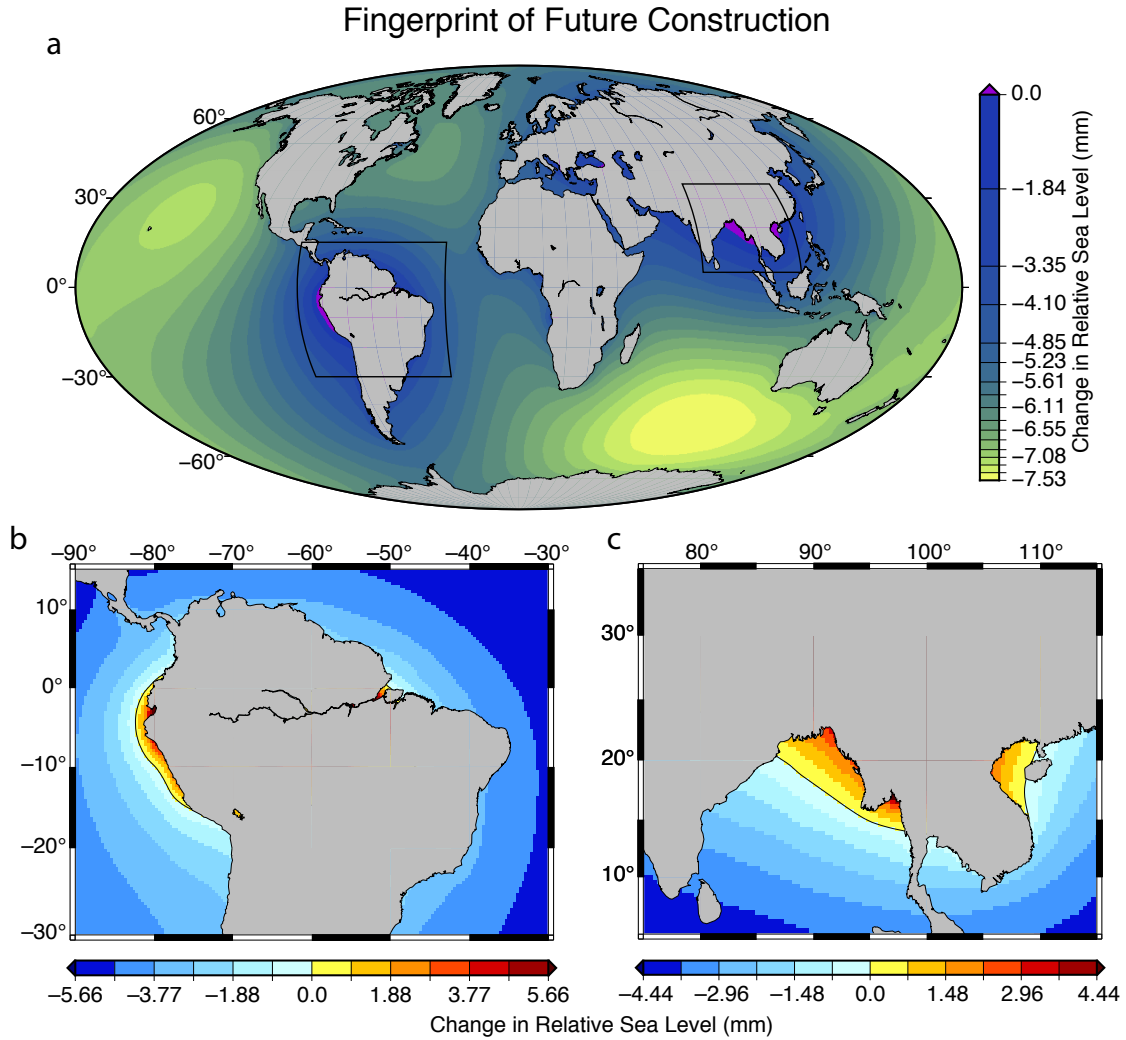
Figure 4. Relative sea level change computed using all reservoirs in the Zarfl *et al.* (2015) database, assumed to be completed by 2040, with seepage included as described in the text. (**a**) Global GRD fingerprint signal. Colors as in Fig. 3. (**b**) Detail of frame (**a**) in South America, showing sea level rise of a few mm along the west coast of Ecuador and Peru and around the mouth of the Amazon River in Brazil. Cool colors show sea level fall; warm colors show sea level rise. (**c**) Detail of frame (**a**) in Southeast Asia, indicating sea level rise of a few mm along the low-lying coasts of Bangladesh and Myanmar, and 1–2 mm along the Vietnamese coast along the Gulf of Tonkin.

4 Discussion

4.1 *Tide Gauge Observations*

Our time series provides a globally resolved estimate of the yearly change in sea level from 1900 – 2011 due to the construction of reservoirs. Tide gauges record local changes in sea level, which may show the effect of reservoir construction. Because of the variability in sea level recorded in tide gauge data, only the largest, most rapid changes will be visible. These are likely to be not the result of sustained building of reservoirs over time, but rather a tide gauge's

236 proximity to a single large reservoir. To determine whether any of these changes are resolvable
237 in the tide gauge record, we first calculate the maximum yearly rate of change predicted at each
238 tide gauge site in the Permanent Service for Mean Sea Level (PSMSL) revised local reference
239 (RLR) database (http://www.psmsl.org/data/obtaining/; Holgate *et al*., 2013), shown in Fig. 5a.
240 The largest predicted changes in sea level due to water impoundment are in northern Europe,
241 Ghana, Malaysia, and the Saint Lawrence Seaway in Canada, all of which have tide gauges in
242 close proximity (< 200 km) to the construction of a single large reservoir.

243   We begin by correcting the tide gauge data using two barotropic ocean circulation models
244 (Piecuch *et al*., 2019). These models predict sea surface height from surface wind stress and air
245 pressure records from two forcing datasets, ERA-20C (Poli *et al*., 2013) and NOAA-20CRv2
246 (Compo *et al*., 2011), and extend throughout the 20th century. At each tide gauge location, we
247 subtract the annual average sea surface height derived in these models at each candidate tide
248 gauge location from the raw tide gauge data to remove the atmospheric contribution from the sea
249 level records. We then compare the atmospheric-corrected sea level time series to our predicted
250 changes due to historical impoundment, focusing on locations where we predict that the largest
251 water impoundment-induced signals occurred.

252   The largest predicted rates of change due to impoundment occur at two tide gauges in the
253 St. Lawrence River in Canada, Baie-Comeau and Point-au-Père/Rimouski. The filling of the
254 Manicouagan reservoir from 1968 – 1974 is predicted to have caused a sea level rise at these
255 sites of almost 40 mm over six years (more than 6 mm yr^{-1}, which is more than 7 times the
256 GMSL rise over this period, 0.8 mm yr^{-1}; Dangendorf *et al*., 2019) The expected, observed, and
257 corrected tide gauge records are shown in Fig. 5b–c. There is too much variability in the
258 observations to confidently detect the signal associated with the construction of the Manicouagan
259 reservoir in the tide gauge data. In any case, the St. Lawrence River is a controlled waterway, so
260 the impoundment signal in the record may be muted or entirely absent. Other sites were either
261 not in operation at the right time (*e.g*., Stenungsund, Sweden; Tema, Ghana; and Cendering,
262 Malaysia). Candidate tide gauge predictions and observations are shown in Fig. S3. A more
263 complete characterization of sea level behavior, whether through using a variety of ocean
264 reanalysis models (Chepurin *et al*., 2014) or more sophisticated modeling techniques (Piecuch *et*
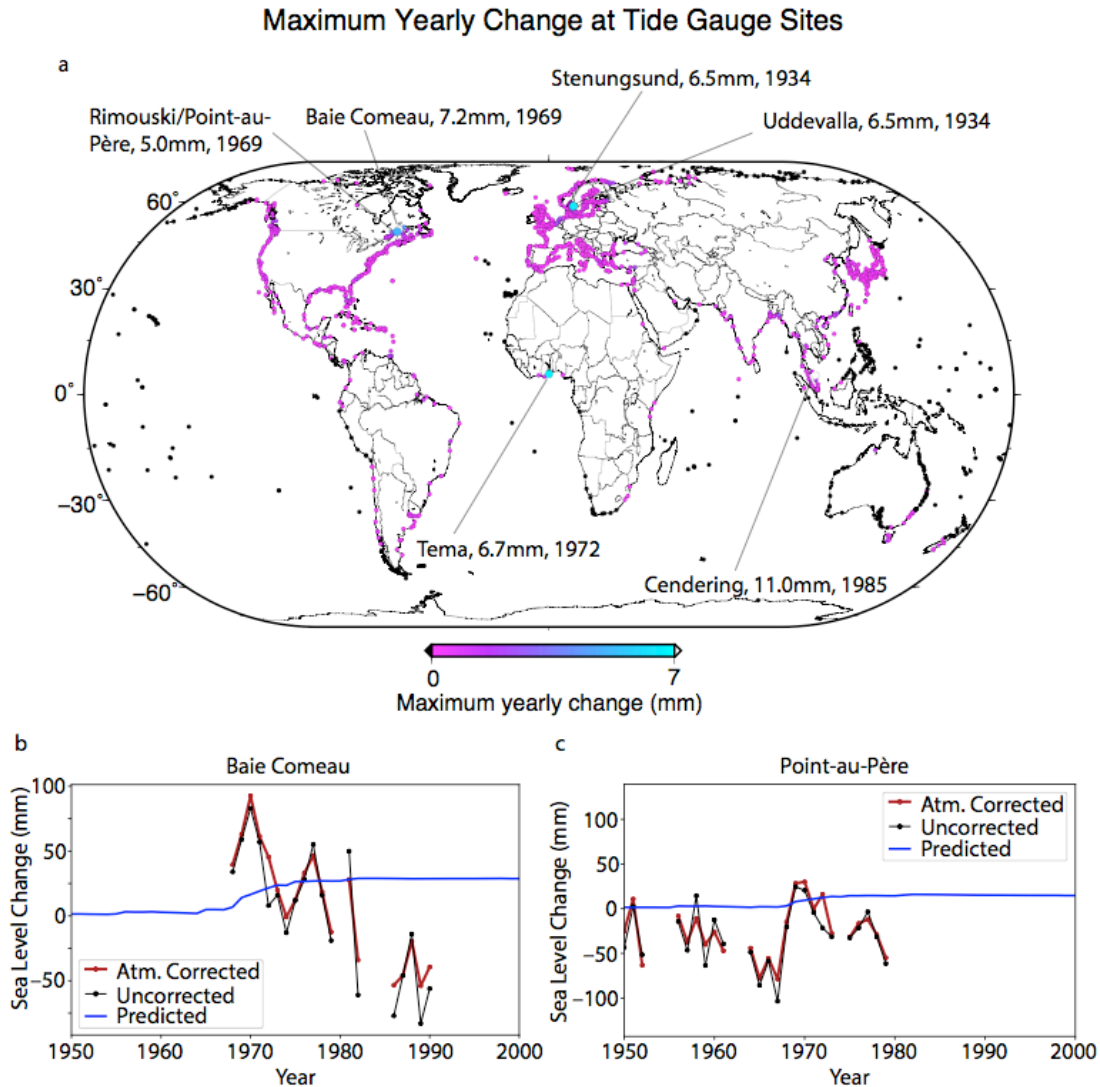265 *al*., 2017), may resolve an impoundment signal in tide gauge data sets.

Figure 5. Tide gauge predictions and observations. (**a**) Maximum yearly change at each PSMSL RLR tide gauge site. Six sites have a predicted a maximum yearly change of 5 mm or more. These six sites are distinguished by a larger symbol; also indicated are the tide gauge name, the maximum predicted yearly increase, and the year in which that maximum occurred. (**b**) Predicted sea level change due to reservoir construction (blue) versus RLR PSMSL observed (black dots) and atmospheric corrected sea level (Piecuch *et al.*, 2019; red points) at the Baie Comeau, Québec, Canada tide gauge, near the Manicouagan Reservoir. The reservoir was filled from 1970 to 1978. Units on the vertical axis are millimeters, but the absolute value is arbitrary. (**c**) As in (**b**), but for tide gauge in Point-au-Père, Québec, Canada.

4.2 *Variability in Reservoir Storage*

Seepage is not the only mechanism that can alter the mass of a reservoir after impoundment. An additional post-construction signal comes from variations in the amount of

281   water impounded, either seasonally, or in long-term draw-down of the water. We assess both of
282   these for a handful of the largest reservoirs. Records of lake levels can be difficult to obtain in a
283   uniform manner, so we use changes in the surface height as observed by satellite altimetry,
284   provided by the USDA Global Reservoir and Lake Elevation Database
285   (https://ipad.fas.usda.gov/cropexplorer/global_reservoir/) to estimate the mass change. The
286   satellites generally observed the largest reservoirs two to three times a month, beginning in 1992
287   and continuing through the study period. Because fluctuations in lake level are small over the
288   ~10-day timescale between satellite observations, the behavior of the reservoir volume can be
289   reasonably well constrained by this method. Dramatic increases of impounded water that happen
290   over a shorter timescale are generally due to large precipitation events, in which case the signal
291   from the reservoir is likely to be masked by a significant increase in groundwater and surface
292   water unrelated to the reservoir itself.

293   From the surface area and volume provided for each reservoir in the GRanD database we
294   calculate a mean depth. The altimetry data show changes in altitude, but not absolute altitude, so
295   we cannot use these data to verify when the reservoir is full. Instead, we set the maximum datum
296   from the altimetry as the mean depth of the reservoir, assuming that this represents a full
297   reservoir. We then use every other altimetric data point to estimate the fractional change of the
298   mean depth, and approximate this as the fractional change of the volume of the reservoir. We
299   discuss both long-term drawdown and seasonal changes in water storage.

300   Lake Powell in the United States is an excellent target for detailed investigation. First,
301   high-resolution data are available to verify the accuracy of the GRanD dataset. Second, satellite
302   altimetry data show that Lake Powell is characterized by a decline in lake level of slightly more
303   than 12 m between 2000 and 2011. Therefore, we can use the data set to investigate the effects of
304   a long-term reduction in water storage, and whether the use of satellite altimetry is appropriate in
305   determining storage changes in large reservoirs.

306   GRanD lists Lake Powell as the 43rd largest reservoir in the database, with a capacity of
307   25.07 km^3 and a surface area of 120.7 km^2. In contrast, the Bureau of Reclamation (BoR; part of
308   the United States Department of the Interior), which manages Lake Powell and the Glen Canyon
309   Dam that impounds it, lists the capacity as 32.3 km^3 and the surface area as 688.9 km^2
310   (https://www.usbr.gov/uc/rm/crsp/gc/). These two sets of estimates produce very different values
311   for the mean depth of the reservoir, 208 m and 47 m respectively. The 12 m decline shown in the
312   satellite altimetry data, then, represents a reduction in impounded water of either 6% or 25%.
313   The BoR also provide daily calculations of reservoir storage based on the observed elevation of
314   the water level and bathymetric surveys. For the time period 2000 to 2011, these surveys
315   (https://www.usbr.gov/rsvrWater/HistoricalApp.html) indicate that the elevation in Lake Powell
316   decreased 13 m from 1122 m to 1109 m, and that storage in Lake Powell decreased from 27.1
317   km^3 to 19.7 km^3, a decrease of 27%. The satellite altimetry data are thus consistent with the
318   water impoundment reported by the BoR, and additionally support the BoR-reported parameters
319   for reservoir size, rather than the values in the GRanD database.

320   While a decline of 27% in the volume of the reservoir does contribute meaningfully to
321   the GRD fingerprint through time, it is similar in magnitude—but opposite in sign—to the
322   seepage we assume for Lake Powell (Fig. S4b). This time series indicates that significant, long-
323   term drawdown in impoundment can change the magnitude of local sea level change associated
324   with the unloading. However, for reservoirs that do not experience significant drawdown in
325   storage, periods of low water levels will be characterized by a relatively small perturbation in

326 local sea level, and will have a second-order effect on the global fingerprint of artificially
327 impounded water.

328   Lake Guri, a reservoir in Venezuela with a volume of 135 km^3, experiences seasonal
329 variations in surface height that routinely exceed 10 m, representing almost 30% of the
330 reservoir's capacity as calculated from the GRanD-reported volume and surface area. We
331 compare sea level predictions—those that do and do not include variability in Lake Guri—at the
332 closest grid point to Lake Guri at in Fig. S4a. Note that this location is not on the coast; because
333 the coast is at a greater distance, the impoundment signal will be smaller there. The perturbations
334 in sea level in this case are on the order of a few millimeters, with higher sea level occurring
335 when the reservoir is full, as expected. If the seasonality is due to precipitation, *i.e.*, a full
336 reservoir occurs during a rainy season, then GRD effects associated with the higher level of
337 impoundment could enhance the hazard of coastal flooding at precisely the time when increasing
338 rain makes flooding more likely.

339   4.3 *Future Changes in Sea Level*

340   Our projections of future changes in sea level due to water impoundment are significantly
341 larger than previous estimates. Following Rahmstorf *et al.*, (2012), Kopp *et al.* (2014) use
342 impoundment data from the WRD (Chao *et al.*, 2008) and population projections from the
343 United Nations Department of Economics and Social Affairs (2013) to derive a relationship
344 between cumulative impoundment and population (see Supporting Information); their analysis
345 implies a maximum additional water impoundment corresponding to an additional GMSL fall of
346 6 mm. We plot the future construction suggested by Zarfl *et al.* (2015) alongside this relationship
347 in Fig. S5, and show that the extrapolation to 2040 based on Kopp *et al.* (2014) underestimates
348 impoundment by 8.4 mm equivalent GMSL fall. There are uncertainties in our estimates based
349 on the Zarfl *et al.* (2015) database. However, it is clear that the previously derived relationship
350 between cumulative impoundment and world population is likely to significantly underestimate
351 future artificial impoundment contributions to sea level changes.

352   Finally, we show in detail predictions for two areas that the Zarfl *et al.* (2015) database
353 indicates will experience significant increases in reservoir impoundment: Southeast Asia and
354 southeastern Brazil (Fig. 4). These relatively low-elevation, highly populated areas near the coast
355 will experience a sea level rise due to impoundment of as much as ~10 mm in the next two
356 decades that will enhance the hazard associated with global mean sea level rise. Vitousek *et al.*
357 (2017) suggest that in tropical areas, sea level rise of as little as 50 mm can double the coastal
358 flooding hazard. Thus, major reservoir construction near such coasts could change the frequency
359 of flooding in these populated areas.

360 **5 Conclusions**

361   We present an estimate of spatially and temporally resolved sea level change due to the
362 impoundment of water in artificial reservoirs from 1900 to 2011, and a projection of sea level
363 change to the year 2040 due to the same effects. For each year over the period 1900 – 2011, our
364 predicted global GRD fingerprints are available by download from
365 doi.org/10.5281/zenodo.3751986.

366   Our analysis of historical data (Lehner *et al.*, 2011) is consistent with previous studies
367 (Chao *et al.*, 2008; Fiedler and Conrad, 2010) that have estimated that globally averaged sea
368 level fell between 21 mm and 30 mm over the course of the twentieth century, representing a

369 significant fraction of the sea level budget. Our spatial analysis is generally consistent with
370 previous work (Fiedler and Conrad, 2010), but the spatio-temporal resolution of the predictions
371 we present allows for comparison of predictions to records from specific tide gauge sites. Our
372 estimate that reservoir impoundments could have raised sea level by as much as 40 mm should
373 motivate such studies.

374 Our analysis of reservoirs that are in some form of planning or construction (Zarfl *et al.*,
375 2015) shows that the era of reservoir construction has not ceased, that this continued
376 impoundment will contribute significantly to changes in sea level, and that the spatial pattern of
377 sea level change will be different from that of the majority of the twentieth century. We show
378 that current best projections may underestimate by nearly a centimeter the effect of water
379 impoundment on GMSL in the next 20 years. It is difficult to accurately predict the sea level
380 fingerprint of reservoirs without precise estimates of the volumetric capacity. Nonetheless, our
381 calculations demonstrate that in areas characterized by a high density of reservoir construction,
382 artificial impoundment is predicted to cause a local rise in sea level, which may change the
383 hazard of coastal flooding. This suggests that an analysis of the local effects on sea level should
384 be performed prior the impoundment of large volumes of water in tropical areas of low elevation,
385 including Southeast Asia and southeastern Brazil.

386 Finally, our study highlights the importance of establishing a comprehensive database of
387 water impoundment that is volumetrically complete, and geospatially and temporally referenced.
388 Artificial water impoundment is a crucial piece of the sea level budget (Cazenave *et al.*, 2018;
389 Kopp *et al.*, 2014, 2015), and accurately accounting for its spatially and temporally varying
390 contribution is imperative. The database would be important not only for the community
391 concerned with the impacts of sea level rise, but also to a number of others, including those
392 focused on assessments of global electricity generation (Zarfl *et al.*, 2015), the impact of river
393 fragmentation on ecosystems (Grill *et al.*, 2015), and hazards related to reservoir-induced
394 seismicity (*e.g.*, Gupta, 2002). In the absence of such a database, our analysis represents the most
395 complete estimate to date of sea level change due to artificial impoundment of water from 1900
396 to 2040.

397 **Acknowledgments, Samples, and Data**

408 **References**

409 Cazenave, A., & WCRP Global Sea Level Budget Group (2018). Global sea-level budget 1993–
410 present. *Earth System Science Data*, *10*(3), 1551–1590. https://doi.org/10.5194/essd-10-1551-
411 2018

412 Chao, B. F., Wu, Y. H., & Li, Y. S. (2008). Impact of artificial reservoir water impoundment on
413 global sea level. *Science*, *320*(5873), 212–214. https://doi.org/10.1126/science.1154580

414 Chepurin, G. A., Carton, J. A., & Leuliette, E. (2014). Sea level in ocean reanalyses and tide
415 gauges. *Journal of Geophysical Research: Oceans*, *119*(1), 147–155.
416 https://doi.org/10.1002/2013JC009365

417 Compo, G. P., Whitaker, J. S., Sardeshmukh, P. D., Matsui, N., Allan, R. J., Yin, X., et al.
418 (2011). The Twentieth Century Reanalysis Project. *Quarterly Journal of the Royal*
419 *Meteorological Society*, *137*(654), 1–28. https://doi.org/10.1002/qj.776

420 Dangendorf, S., Hay, C., Calafat, F. M., Marcos, M., Piecuch, C. G., Berk, K., & Jensen, J.
421 (2019). Persistent acceleration in global sea-level rise since the 1960s. *Nature Climate Change*,
422 *9*(9), 705–710. https://doi.org/10.1038/s41558-019-0531-8

423 Dziewonski, A. M., & Anderson, D. L. (1981). Preliminary reference Earth model. *Physics of the*
424 *Earth and Planetary Interiors*, *25*(4), 297–356. https://doi.org/10.1016/0031-9201(81)90046-7

425 Fiedler, J. W., & Conrad, C. P. (2010). Spatial variability of sea level rise due to water
426 impoundment behind dams. *Geophysical Research Letters*, *37*(12), 1–6.
427 https://doi.org/10.1029/2010GL043462

428 Gregory, J. M., Griffies, S. M., Hughes, C. W., Lowe, J. A., Church, J. A., Fukimori, I., et al.
429 (2019). Concepts and Terminology for Sea Level: Mean, Variability and Change, Both Local and
430 Global. *Surveys in Geophysics*, *40*(6), 1251–1289. https://doi.org/10.1007/s10712-019-09525-z

431 Grill, G., Lehner, B., Lumsdon, A. E., MacDonald, G. K., Zarfl, C., & Reidy Liermann, C.
432 (2015). An index-based framework for assessing patterns and trends in river fragmentation and
433 flow regulation by global dams at multiple scales. *Environmental Research Letters*, *10*(1),
434 015001. https://doi.org/10.1088/1748-9326/10/1/015001

435 Gupta, H. K. (2002). A review of recent studies of triggered earthquakes by artificial water
436 reservoirs with special emphasis on earthquakes in Koyna, India. *Earth-Science Reviews*, *58*(3–
437 4), 279–310. https://doi.org/10.1016/S0012-8252(02)00063-6

438 Harr, M. E. (Ed.). (1962). *Groundwater and Seepage*. New York: McGraw-Hill.

439 Holgate, S. J., Matthews, A., Woodworth, P. L., Rickards, L. J., Tamisiea, M. E., Bradshaw, E.,
440 et al. (2013). New Data Systems and Products at the Permanent Service for Mean Sea Level.
441 *Journal of Coastal Research*, *288*, 493–504. https://doi.org/10.2112/JCOASTRES-D-12-00175.1

442 Kendall, R. A., Mitrovica, J. X., & Milne, G. A. (2005). On post-glacial sea level - II. Numerical
443 formulation and comparative results on spherically symmetric models. *Geophysical Journal*
444 *International*, *161*(3), 679–706. https://doi.org/10.1111/j.1365-246X.2005.02553.x

445 Kopp, R. E., Horton, R. M., Little, C. M., Mitrovica, J. X., Oppenheimer, M., Rasmussen, D. J.,
446 et al. (2014). Probabilistic 21st and 22nd century sea-level projections at a global network of
447 tide-gauge sites. *Earth's Future*, *2*(8), 383–406. https://doi.org/10.1002/2014ef000239

448 Kopp, R. E., Hay, C. C., Little, C. M., & Mitrovica, J. X. (2015). Geographic Variability of Sea-
449 Level Change. *Current Climate Change Reports*, *1*(3), 192–204. https://doi.org/10.1007/s40641-
450 015-0015-5

451 Lehner, B., Liermann, C. R., Revenga, C., Vörösmarty, C. J., Fekete, B. M., Crouzet, P., Döll, P.,
452 Endejan, M., & Frenken, K. (2011). Global Reservoir and Dam (GRanD) database. *European*
453 *Environment*, (March), 12. https://doi.org/10.7927/H4HH6H08

454 Lehner, B., Liermann, C. R., Revenga, C., Vörösmarty, C. J., Fekete, B. M., Crouzet, P., Döll, P.,
455 Endejan, M., Frenken, K., et al. (2011). High-resolution mapping of the world's reservoirs and
456 dams for sustainable river-flow management. *Frontiers in Ecology and the Environment*, *9*(9),
457 494–502. https://doi.org/10.1890/100125

458 Loo, T. (2007). Disturbing the Peace: Environmental Change and the Scales of Justice on a
459 Northern River. *Environmental History*, *12*(4), 895–919. https://doi.org/10.1093/envhis/12.4.895

460 Mitrovica, J.X. & Milne, G.A. (2003). On post-glacial sea level: I. General theory. *Geophys. J.*
461 *Int., 154*, 253-267.

462 Mitrovica, J.X., Gomez, N., Morrow, E., Hay, C., Latychev, K. , & Tamisiea, M.E. (2011). On
463 the robustness of predictions of sea-level fingerprints. *Geophys. J. Int., 187*, 729-742.

464 Piecuch, C. G., Calafat, F. M., Dangendorf, S., & Jordà, G. (2019). *The Ability of Barotropic*
465 *Models to Simulate Historical Mean Sea Level Changes from Coastal Tide Gauge Data. Surveys*
466 *in Geophysics* (Vol. 40). Springer Netherlands. https://doi.org/10.1007/s10712-019-09537-9

467 Piecuch, C. G., Huybers, P., & Tingley, M. P. (2017). Comparison of full and empirical Bayes
468 approaches for inferring sea-level changes from tide-gauge data. *Journal of Geophysical*
469 *Research: Oceans*, *122*(3), 2243–2258. https://doi.org/10.1002/2016JC012506

470 Poli, P., Hersbach, H., Tan, D., Dee, D., Thépaut, J.-N., Simmons, A., et al. (2013). The data
471 assimilation system and initial performance evaluation of the ECMWF pilot reanalysis of the
472 20th-century assimi- lating surface observations only (ERA-20C). ERA Report series 14.

473 Rahmstorf, S., Perrette, M., & Vermeer, M. (2012). Testing the robustness of semi-empirical sea
474 level projections. *Climate Dynamics*, *39*(3–4), 861–875. https://doi.org/10.1007/s00382-011-
475 1226-7

476 Vitousek, S., Barnard, P. L., Fletcher, C. H., Frazer, N., Erikson, L., & Storlazzi, C. D. (2017).
477 Doubling of coastal flooding frequency within decades due to sea-level rise. *Scientific Reports*,
478 *7*(1), 1399. https://doi.org/10.1038/s41598-017-01362-7

479 Vörösmarty, C. J., Sharma, K. P., Fekete, B. M., Copeland, A. H., Holden, J., Marble, J., &
480 Lough, J. A. (1997). The Storage and Aging of Continental Runoff in Large Reservoir Systems
481 of the World. *Ambio*, *26*(4), 210–219.

482 Wessel, P., Smith, W. H. F., Scharroo, R., Luis, J., & Wobbe, F. (2013). Generic Mapping Tools:
483 Improved Version Released. *Eos, Transactions American Geophysical Union*, *94*(45), 409–410.
484 https://doi.org/10.1002/2013EO450001

485 United Nations, Department of Economic and Social Affairs, Population Division (2013). World
486 Population Prospects: The 2012 Revision, Highlights and Advance Tables. Working Paper No.
487 ESA/P/WP.228.

488 Zarfl, C., Lumsdon, A. E., Berlekamp, J., Tydecks, L., & Tockner, K. (2015). A global boom in
489 hydropower dam construction. *Aquatic Sciences*, *77*(1), 161–170.
490 https://doi.org/10.1007/s00027-014-0377-0